The EUMETSAT Network of Satellite Application Facilities

O3M SAF
Ozone and Atmospheric Chemistry Monitoring

ALGORITHM THEORETICAL BASIS DOCUMENT

Offline UV (OUV) Products

Prepared by: Jukka Kujanpää Finnish Meteorological Institute

Introduction to EUMETSAT Satellite Application Facility on Ozone and Atmospheric Chemistry Monitoring (O3M SAF)

Background

The need for atmospheric chemistry monitoring was first realized when severe loss of stratospheric ozone was detected over the Polar Regions. At the same time, increased levels of ultraviolet radiation were observed.

Ultraviolet radiation is known to be dangerous to humans and animals (causing e.g. skin cancer, cataract, immune suppression) and having harmful effects on agriculture, forests and oceanic food chain. In addition, the global warming - besides affecting the atmospheric chemistry - also enhances the ozone depletion by cooling the stratosphere. Combined, these phenomena have immense effects on the whole planet. Therefore, monitoring the chemical composition of the atmosphere is a very important duty for EUMETSAT and the world-wide scientific community.

Objectives

The main objectives of the O3M SAF are to process, archive, validate and disseminate atmospheric composition products (O_3, NO_2, SO_2, OClO, HCHO, BrO, H_2O), aerosols and surface ultraviolet radiation utilising the satellites of EUMETSAT. The majority of the O3M SAF products are based on data from the GOME-2 spectrometer onboard MetOp-A satellite.

Another important task of the O3M SAF is the research and development in radiative transfer modelling and inversion methods for obtaining long-term, high-quality atmospheric composition products from the satellite measurements.

Product families

- Near real-time Total Column (NTO)
  - O_3, NO_2, O_3Tropo, NO_2Tropo
- Near real-time Ozone Profile (NOP)
- Near real-time UV Index (NUV)
- Offline Total Column (OTO)
  - O_3, NO_2, O_3Tropo, NO_2Tropo, SO_2, BrO, H_2O, HCHO, OClO
- Offline Ozone Profile (OOP)
- Offline Surface UV (OUV)
- Aerosols (ARS)

Product timeliness and dissemination

Data products are divided in two categories depending on how quickly they are available to users:

Near real-time products are available in less than three hours after measurement. These products are disseminated via EUMETCast (NTO, NOP), GTS (NTO, NOP) or Internet (NUV).

Offline products are available in two weeks from the measurement and they are archived at the O3M SAF archives in Finnish Meteorological Institute (OOP, OUV, ARS) and German Aerospace Center (OTO).

Only products with “pre-operational” or “operational” status are disseminated. Up-to-date status of the products and ordering info is available on the O3M SAF website.

Information about the O3M SAF project, products and services: http://o3msaf.fmi.fi/

O3M SAF Helpdesk: o3msaf@fmi.fi

DOCUMENT STATUS SHEET

Issue	Date	Modified items / Reason for change
1.0	26.03.2007	Initial revision of the full document
1.1	04.04.2008	rewrote the whole document
1.2	15.09.2008	Updated according to ORR-A3 RIDs. o3m_atbd_ouv_i1r1_20080404_Munro_010, 2.1/1/5: - added ref. to VLIDORT Model o3m_atbd_ouv_i1r1_20080404_Munro_011, 4.6/-/15: - added the condition albedo < 0.8 to the statement on the 50 % threshold. OUV_ATBD_Lang_01: 2.1/-/6 - added explanation to the factor 40 and a reference
1.3	20.05.2013	Updated for PCR -added vitamin D weighting -removed SCUP-h weighting -added computation of photolysis frequencies -introduced the homogenized cover page -added the SAF introduction
1.4	28.06.2013	- sect. 1.2: added acronyms - eq. 2.7: replaced h with z and added a description: z is the height from the surface. - eq. 2.10: corrected for O(3P) and added description: The Planck constant is denoted by h. - eq. 3.3: added: i_w is the index of the weighting function -table 2.1: swapped wavelength ranges of UVA and UVB - sect. 3.1.: added refs to aerosol and surface albedo climatologies - sect. 3.: - added new table 3.1, clarified table 3.2 (previously 3.1), added table 3.3. - sect. 4, par. 1: added comment on the applicability of the error analysis to all products - sect 4.2.: added comment on the selection of 5 % error for surface albedo - added sect. 1.4: Product overview - sect. 2.3: added comment on AVHRR pixels vs. surface grids - added sects. 2.4 on auxiliary data and 2.5 on diurnal integral

Contents

1 INTRODUCTION

1.1 Purpose and scope

This document is the algorithm theoretical basis document of the O3M SAF Offline UV product (OUV).

1.2 Acronyms

AERONET	AErosol RObotic NETwork
AOD	Aerosol Optical Depth
ARS	Aerosol Retrieval System / Aerosol product
ATBD	Algorithm Theoretical Basis Document
ATLAS-3	Atmospheric Laboratory for Applications and Science-3 (a space shuttle)
AVHRR	Advanced Very High Resolution Radiometer
BRDF	Bidirectional Reflectance Distribution Function
CIE	Commission Internationale de l'Éclairage, International Commission on Illumination
COD	Cloud optical depth
DEM	Digital Elevation Model
DNA	Deoxyribonucleic acid
DSR	Dose rate
ERS-2	European Remote-Sensing Satellite-2
EUMETCast	EUMETSAT's broadcast system for environmental data
EUMETSAT	European Organisation for the Exploitation of Meteorological Satellites
FMI	Finnish Meteorological Institute
GADS	Global Aerosol Data Set
GAC	Global Area Coverage
GOME-2	Global Ozone Monitoring Experiment-2
GTOPO30	Global 30 Arc Second Elevation Data Set
GTS	Global Telecommunications System
HDF	Hierarchial Data Format
Internet	International network
LAC	Local Area Coverage
LUT	Look-up table
Metop	Meteorological Operational satellite programme
MLER	Minimum Lambert Equivalent Reflectivity
NOAA	National Oceanic and Atmospheric Administration
NOP	Near real-time Ozone Profile product
NRT	Near real-time
NTO	Near real-time Total Ozone product
NUV	Near real-time UV product
O3M SAF	Satellite Application Facility on Ozone and Atmospheric Chemistry Monitoring
OOP	Offline Ozone Profile product
OTO	Offline Total Ozone product
OUV	Offline UV product
RMS	Root Mean Square
SUSIM	Solar Ultraviolet Spectral Irradiance Monitor
TOMS	Total Ozone Mapping Spectrometer
UV	Ultraviolet radiation
UVI	UV Index
VLIDORT	Linearized pseudo-spherical Vector Discrete Ordinate Radiative Transfer code
WHO	World Health Organization

1.3 References

1.3.1 Applicable Documents

[AD1] O3M SAF Product Requirements Document, SAF/O3M/FMI/RQ/PRD/001, Issue 1.3, 16.5.2013.

1.3.2 Reference Documents

[RD1] Global Solar UV Index: A Practical Guide, WHO, 2002, ISBN 92 4 159007 6, Annex C, http://www.who.int/uv/publications/en/GlobalUVI.pdf

[RD2] McKinlay A.F and Diffey B.L., *CIE Research Note*, 6(1), 1987

[RD3] Setlow R.B., *Proc. Nat. Acad. Sci. USA.*, 71, 3363-3366, 1974.

[RD4] Caldwell, M.M. "Solar UV Irradiation and the Growth and Development of Higher Plants", pages 131-177 in Giese A.G (ed.) *Photophysiology*, vol 6. Academic Press, New York, 1971

[RD5] CIE, 2006. Action spectrum for the production of previtamin D3 in human skin. Technical Report 174. International Commission on Illumination.

[RD6] Koepke, P., M. Hess, I. Schult, and E.P. Shettle (1997): Global Aerosol Data Set, Report No. 243, Max-Planck-Institut für Meteorologie, Hamburg, ISSN 0937-1060.

[RD7] Deirmendjian, D.: Electromagnetic Scattering on Spherical Polydispersions, American Elsevier Publishing Company, Inc., New York, 1969.

[RD8] Spurr, R.J.D, "VLIDORT: A linearized pseudo-spherical vector discrete ordinate radiative transfer model for forward model and retrieval studies in multilayer multiple scattering media." *J. Quant. Spectrosc. Radiat. Transfer*, doi:10.1016/j.jqsrt.2006.05.005, 2006

[RD9] Krotkov, N. A., Bhartia, P. K., Herman, J. R, Fioletov, V. and Kerr, J., "Satellite estimation of spectral surface UV irradiance in the presence of tropospheric aerosols 1: Cloud-free case." *J. Geophys. Res.* 103, 8779, 1998

[RD10] Krotkov, N. A., Herman, J. R, Bhartia, P. K, Fioletov, V. and Ahmad, Z., "Satellite estimation of spectral surface UV irradiance 2. Effects of homogeneous clouds and snow", *J. Geophys. Res.* 106, 11743-11759, 2001

[RD11] Meerkötter, R. and Bugliaro L., "Synergethic use of NOAA/AVHRR and Meteosat cloud information for space based UV measurements", *Proc. SPIE*, vol. 4482, 169-176, 2002.

[RD12] Eck T.F., P.K. Bhartia and J.B. Kerr, "Satellite estimation of spectral UVB irradiance using TOMS derived total ozone and UV reflectivity.", *Geophys. Res. Lett.*, 22, 611-614, 1995

[RD13] Herman, J.R., and E. Celarier, "Earth surface reflectivity climatology at 340-380 nm from TOMS data." *J. Geophys. Res.*, 102, 28,003-28,011, 1997.

[RD14] DeMore, W.B., S.P. Sander, D.M. Golden, R.F. Hampson, M.J. Kurylo, C.J. Howard, A.R. Ravishankara, C.E. Kolb, and M.J. Molina, "Chemical Kinetics and Photochemical Data for Use in Stratospheric Modeling", Evaluation No. 12, Jet Propulsion Laboratory, Publication 97-4, Pasadena, CA, 1997.

[RD15] Talukdar, R. K., C.A. Langfellow, M.K. Gilles, and A.R. Ravishankara, "Quantum yields of $O(^1D)$ in the photolysis of ozone between 289 and 329 nm as a function of temperature", *Geophys. Res. Lett.*, 25, 143-146, 1998.

[RD16] Schneider, W., G.K. Moortgat, J.P. Burrows, and G.S. Tyndall, "Absorption cross-sections of NO2 in the UV and visible region (200 - 700 nm) at 298 K", *J. Photochem. Photobiol.*, 40, 195-217 (1987).

[RD17] Brion, J., A. Chakir, D. Daumont, and J. Malicet, "High-resolution laboratory absorption cross section of O3. Temperature effect", *Chem. Phys. Lett.*, 213 (5-6), 610-512, 1993.

[RD18] Brion, J., A. Chakir, J. Charbonnier, D. Daumont, C. Parisse, and J. Malicet, "Absorption spectra measurements for the ozone molecule in the 350-830 nm region", *J. Atmos. Chem.*, 30, 291-299, 1998.

[RD19] Daumont, M., J. Brion, J. Charbonnier, and J. Malicet, "Ozone UV spectroscopy I: Absorption cross-sections at room temperature", *J. Atmos. Chem.*, 15, 145-155, 1992.

[RD20] Malicet, J., D. Daumont, J. Charbonnier, C. Parisse, A. Chakir, and J. Brion, "Ozone UV spectroscopy, II. Absorption cross-sections and temperature dependence", *J. Atmos. Chem.*, 21, 263-273, 1995.

[RD21] Kinne S. (2007): Towards an observation-tied AOD climatology, presentation in AT2 Aerosol Workshop, Bremen, June 2007.

[RD22] Tanskanen, A., (2004) Lambertian surface albedo climatology at 360 nm from TOMS data using moving time-window technique. *Proc. XX Quadrennial Ozone Symposium*, 1-8 June, Kos, Greece., pp 1159-1160.

[RD23] Wellemeyer, C. G., S. L. Taylor, C. J. Seftor, R. D. McPeters, and P. K. Bhartia (1997), "A correction for total ozone mapping spectrometer profile shape errors at high latitude", *J. Geophys. Res.*, 102(D7), 9029-9038, doi:10.1029/96JD03965.

1.4 Product overview

The O3M SAF offline surface UV products are derived from the measurements of the operational polar orbiting Metop and NOAA satellites. The products include the most important quantities of the Sun's radiation that can be harmful to life and materials on the Earth. These quantities include daily doses and maximum dose rates of integrated UV-B and UV-A radiation together with values obtained by different biological weighting functions, the solar noon UV index [RD1], and quality control flags. In addition, photolysis frequencies for the photodissosiation of ozone and nitrogen dioxide are given for air quality applications. The products are calculated in a 0.5 degree regular grid and stored in an HDF5 file. The products included in the file are listed in table 1.1 together with their accuracy requirements [AD1]. An example of the daily erythemal dose product is shown in figure 1.1 below.

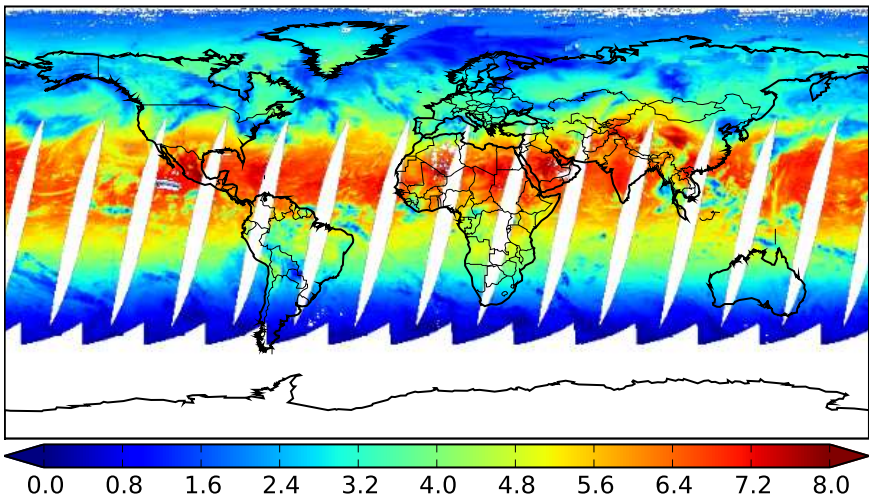

Figure 1.1: An example product field. Erythemal (CIE) daily dose [kJ/m2] on 12 May 2008. The global coverage is limited by the swath of GOME-2 instrument, leaving stripes at low latitudes. The polar night and large solar zenith angles limit the coverage at the winter pole.

Table 1.1: Products stored in the OUV file together with their accuracy requirements.

Product Name	Threshold Accuracy (%)	Target Accuracy (%)	Optimal Accuracy (%)
Offline UV daily dose, erythemal (CIE) weighting	50	20	10
Offline UV daily dose, DNA damage weighting	50	20	10
Offline UV daily dose, plant response weighting	50	20	10
Offline UV daily dose, vitamin D weighting	50	20	10
Offline UV daily dose, UVA weighting	50	20	10
Offline UV daily dose, UVB weighting	50	20	10
Offline UV daily maximum dose rate, erythemal (CIE) weighting	50	20	10
Offline UV daily maximum dose rate, DNA damage weighting	50	20	10
Offline UV daily maximum dose rate, plant response weighting	50	20	10
Offline UV daily maximum dose rate, vitamin D weighting	50	20	10
Offline UV daily maximum dose rate, UVA weighting	50	20	10
Offline UV daily maximum dose rate, UVB weighting	50	20	10
Offline solar noon UV Index	50	20	10
Offline daily maximum ozone photolysis rate	50	20	10
Offline daily maximum nitrogen dioxide photolysis rate	50	20	10

2 Processing algorithm

The overall processing algorithm consists of mapping the GOME-2 total ozone data to a grid, inversion of the cloud optical depth from AVHRR channel 1 reflectances to the same grid, and finally the calculation of surface UV dose rates and daily (integrated) doses. The overall flowchart is shown in figure 2.1 below and the steps are detailed in the following sections.

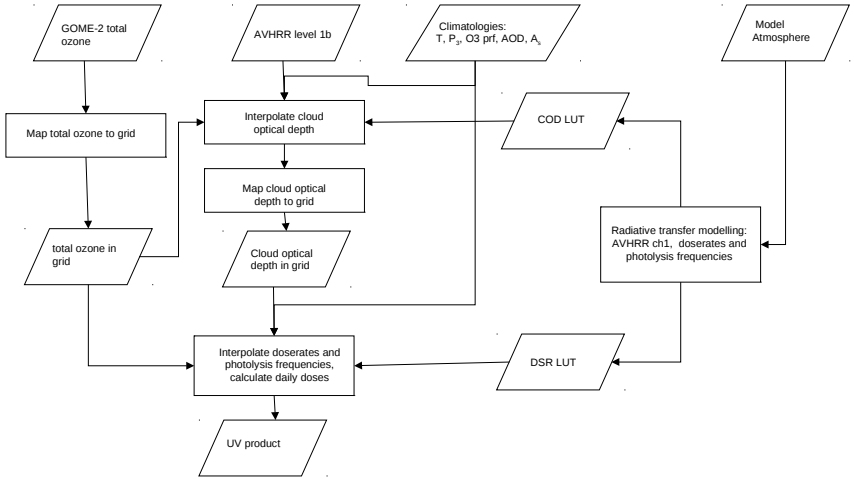

Figure 2.1: Overall processing algorithm. The radiative transfer modelling on the right side of the figure leading to dose rate (DSR LUT, including the photolysis frequencies) and cloud optical depth (COD LUT) look-up tables is done offline and described in chapter 3. The online processing using these look-up tables is described in the sections of this chapter.

2.1 Surface UV dose rates, daily doses and photolysis frequencies

The offline UV product contains surface UV daily doses, daily maximum doserates, solar noon UV index and photolysis frequencies in a regular 0.5x0.5 degree grid [AD1]. Four different biological weighting functions (action spectra) are applied. These weightings are plotted in figure 2.2 and described in table 2.1. First, we calculate the hemispherical spectral irradiance on a horizontal surface $E_h(\lambda)$ using the radiative transfer model VLIDORT [RD8] for computing the downwelling radiance $L(\lambda,\theta,\phi)$ at the surface

$$E_h(\lambda) = \int_0^{2\pi} d\phi \int_0^{\frac{\pi}{2}} L(\lambda,\theta,\phi) cos\theta sin\theta d\theta \tag{2.1}$$

then multiply it by a weighting function $w(\lambda)$ and integrate over the wavelength λ to get the dose rate E'_w

$$E'_w = \int_\lambda w(\lambda) E_h(\lambda) d\lambda \tag{2.2}$$

and then integrate the dose rate over the sunlit part of the day to get the daily dose H_w

$$H_w = \int_{t=sunrise}^{sunset} E'_w(t) dt \tag{2.3}$$

The daily doses obtained from eq. 2.3 for each weighting function of table 2.1 are stored in the product. Also stored are the daily maximum dose rates for each weighting function

$$E'_{w,max} = max(E'_w(t)) \tag{2.4}$$

Table 2.1: Description of the biological weighting functions used in the OUV product.

Weighting function	Ref.	Equation	Integration wavelength range [nm]	Description
CIE	[RD2]	eq. A.1	290 - 400	Measures the reddening of the skin due to sunburn. Also known as the erythemal weighting function. Used for UV index.
DNA	[RD3]	eq. A.2	290 - 400	Measures the ability of UV irradiance to cause damage to unprotected DNA.
Plant	[RD4]	eq. A.3	290 - 400	Measures the generalized response of plants to UV irradiance.
UVB	-	$w = 1$	290 - 315	Integrated UVB radiation
UVA	-	$w = 1$	315 - 400	Integrated UVA radiation
Vitamin D	[RD5]	interpolation of values in table A.1	290 - 330	Vitamin D synthesis

and the solar noon UV index (UVI), obtained by multiplying the CIE weighted dose rate at solar noon in W/m^2 by 40 m^2/W to get a unitless number in a convenient scale [RD1]:

$$UVI = 40E'_{CIE}(t = solar\_noon) \tag{2.5}$$

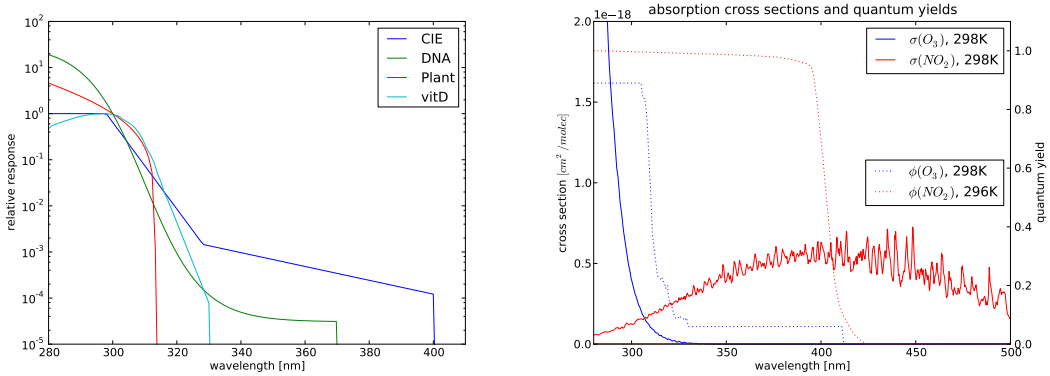

Figure 2.2: Left: the biological weighting functions: CIE (blue), DNA (green), Plant (red) and vitamin D (cyan). Right: cross-sections (solid line) and quantum yields (dotted line) for ozone (blue) and NO_2 (red).

For the photolysis frequencies, the spherical spectral irradiance (actinic flux) $E_s(\lambda)$ at the surface level is computed from

$$E_s(\lambda) = \int_0^{2\pi} d\phi \int_{-\frac{\pi}{2}}^{\frac{\pi}{2}} L(\lambda, \theta, \phi) sin\theta d\theta \tag{2.6}$$

where both downwelling and upwelling radiances are included. Note that there is no $cos\theta$ in the integrand for the spherical irradiance. The photolysis frequency j_x for a species X is obtained by weighting and integrating over wavelength

$$j_x = \int_\lambda \sigma_x(\lambda, T)\phi_x(\lambda, T)E_s(\lambda, \theta_0, z)d\lambda \tag{2.7}$$

where $\sigma_x(\lambda, T)$ is the absorption cross-section and $\phi_x(\lambda, T)$ is the photolysis quantum yield for the species X, T is the temperature and z is the height from the surface. The photolysis frequency is computed for two different species at the surface level ($z = 0$). The rate constant for the formation of atomic oxygen in its exited ^1D state

$$O_3 + h\nu(\lambda < 320nm) \rightarrow O(^1D) + O_2, \quad \frac{d[O(^1D)]}{dt} = j_{O(^1D)}[O_3] \tag{2.8}$$

from ozone is $j_{O(^1D)}$. This is the important photodissosiation route of ozone leading to production of hydroxyl radicals:

$$O(^1D) + H_2O \rightarrow 2OH \tag{2.9}$$

The OH radical thus formed is a key species in various air quality reactions, for example oxidation of

Table 2.2: Parameters for the photolysis frequency calculation.

Species X	Ref. σ_x	Ref. ϕ_x	Integration wavelength range [nm]	Description
$O(^1D)$	[RD17], [RD18], [RD19], [RD20]	[RD15]	290 - 330	photodissosiation of ozone
NO_2	[RD16]	[RD14]	290 - 423	photodissosiation of nitrogen dioxide

hydrocarbons. For the photolysis of nitrogen dioxide

$$NO_2 + h\nu(\lambda < 420nm) \rightarrow NO + O(^3P), \quad -\frac{d[NO_2]}{dt} = j_{NO_2}[NO_2] \tag{2.10}$$

the rate constant is j_{NO_2}. The Planck constant is denoted by h. The atomic oxygen thus formed reacts rapidly with molecular oxygen producing tropospheric ozone and therefore this reaction is also a key reaction related to air quality. The daily maximum values of j_x at the surface level ($z = 0$) are stored in the product.

$$j_{x,max} = max(j_x(t)) \tag{2.11}$$

The references for the absorption cross section and quantum yields are listed in table 2.2. Figure 2.3 shows the flowchart of the dose rate, daily dose and photolysis rate calculation.

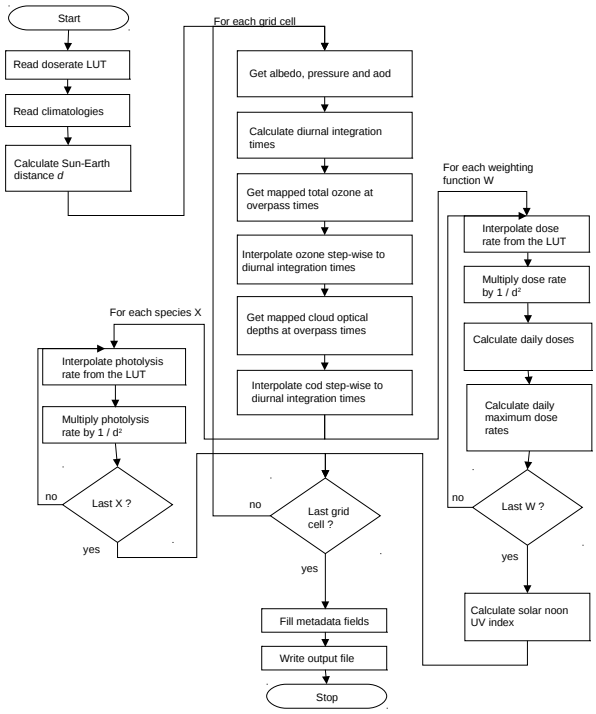

Figure 2.3: Flowchart of the dose rate and daily dose calculation.

2.2 Processing of total ozone data

The surface UV product is derived from GOME-2 near real time total column ozone product (NTO). Total ozone column is used for two different purposes. It accounts for the reduction of the surface UV irradiance by the ozone absorption in the Hartley-Huggins band and for the reduction of the AVHRR channel 1 reflectance by the ozone absorption in the Chappuis band (fig. 2.4). The input NTO data at GOME-2 field of view is mapped to the regular 0.5x0.5 degree grid used in the OUV product as shown in figure 2.5.

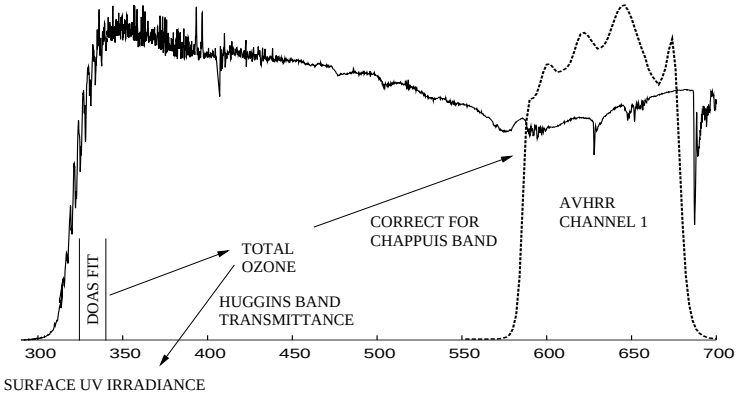

Figure 2.4: GOME/ERS-2 earthshine spectrum (solid line) together with AVHRR/Metop-A channel 1 spectral response function (dotted line) illustrating the use of the input NRT total column ozone product. It accounts both for the Hartley-Huggins band (up to ca. 350 nm) absorption in the surface UV irradiance calculation (280-400 nm) and the Chappuis band absorption (ca. 450-750 nm) in inverting the AVHRR channel 1 reflectance to effective cloud optical depth.

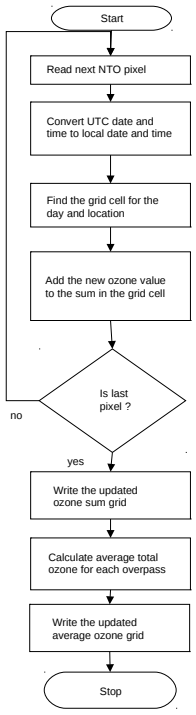

Figure 2.5: Flowchart of the input NTO ozone data processing. Two files are updated during the process: one containing the sum of total ozone and the number of terms in the sum for each overpass of the grid cells while the other one contains the average total ozone for each overpass of the grid cells.

2.3 Estimation of cloud optical depth

Accounting for the effects of clouds is one of the key problems in estimating the daily UV dose from satellite measurements, since cloud data are needed globally with sufficient temporal and spatial resolution to evaluate the diurnal integral (eq. 2.3). Locally, the cloud data are best obtained from the geostationary satellites. However, the OUV product is global, and therefore the data from the AVHRR instrument onboard both Metop and NOAA satellites are used. As Metop is on a morning orbit and NOAA maintaining the afternoon orbit, at least two samples of the diurnal cycle can be obtained globally (fig. 2.6). More overpasses will be available at high latitudes where the instrument swaths overlap for consecutive orbits. This sampling scheme provides a sufficient compromise between the global coverage and sampling of the diurnal cycle. Moreover, the processing data flow can be kept relatively simple as both the Metop and NOAA AVHRR data are available through EUMETCast.

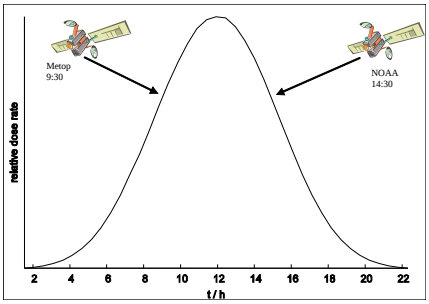

Figure 2.6: The diurnal cycle of UV dose rate (clear-sky case shown for clarity) together with the sampling achieved by Metop and NOAA AVHRR measurements. The sampling of the diurnal cycle is improved at high latitudes where the instrument swaths overlap for consecutive orbits.

The effective cloud optical depth is estimated from the AVHRR channel 1 (centered at ca. 630 nm, see fig. 2.4) reflectance. The reflectance is calculated for model atmospheres using a radiative transfer code, and stored in a look-up table. The effective cloud optical depth is then obtained by interpolating between the calculated values. The Chappuis absorption of ozone (fig. 2.4) is accounted for by using the NRT total column ozone product in the interpolation process. Figure 2.7 shows the flowchart of the cloud optical depth estimation algorithm.

The AVHRR ground pixels are much smaller than the 0.5 x 0.5 degree grid cell used for the surface height and albedo grids (sect. 2.4). The Metop AVHRR level1b data is in Local Area Coverage (LAC) format. The spatial resolution of the LAC data is 1.1 km at nadir. The NOAA AVHRR data are in Global Area Coverage (GAC) format. This is a thinned and averaged version of the LAC format. At nadir, it samples a 3.3 km along track by 5.5 km across track area by a four-pixel average covering 1.1 km along track and 4.4 km across track. In the cloud optical depth retrieval it is assumed that the grid cell is sufficiently homogenous with respect to the surface properties to allow using the 0.5 x 0.5 degree surface property grids for the AVHRR pixels. If the surface properties are too inhomogenous, the cell is flagged with the QC_INHOMOG_SURFACE flag, triggering also the low quality flag. The surface albedo and height grids together with the criteria for inhomogenity are described in section 2.4.

2.4 Auxiliary data grids

2.4.1 Surface height grid

Surface height grid is determined from the U.S. Geological Survey's GTOPO30 digital elevation model (DEM). Elevations in GTOPO30 are regularly spaced at 30-arc seconds (ca. 1 kilometer) and cover the full extent of latitude from 90 degrees south to 90 degrees north, and the full extent of longitude from 180 degrees west to 180 degrees east. Mean height together with the minimum and maximum values are computed from the GTOPO30 map for each 0.5 x 0.5 degree (lat/lon) grid cell. The mean height grid is then used in the cloud optical depth retrieval and in evaluating the surface irradiances. The minimum and maximum height grids are used for quality flagging. If the minimum or maximum height differs from the mean value more than a threshold value for a grid cell, the cell is flagged as inhomogenous by setting the QC_INHOMOG_SURFACE flag on. The threshold value is currently 750 m.

2.4.2 Surface albedo grid

Initially, the Minimum Lambert Equivalent Reflectivity (MLER) climatology [RD13] was used for the surface albedo. However, the MLER fails to properly capture the seasonal changes in albedo during the snow/ice melting and formation periods. A climatology by Tanskanen [RD22] better captures the seasonal effects but contains errors due to cloud contamination. Therefore, the Tanskanen climatology is used for transition periods while the MLER climatology is used elsewhere.

It is assumed that in order for a grid cell to be homogeneous the area defined by the current cell and its nearest neighbouring cells has to be homogenous. The minimum and maximum values of surface albedo

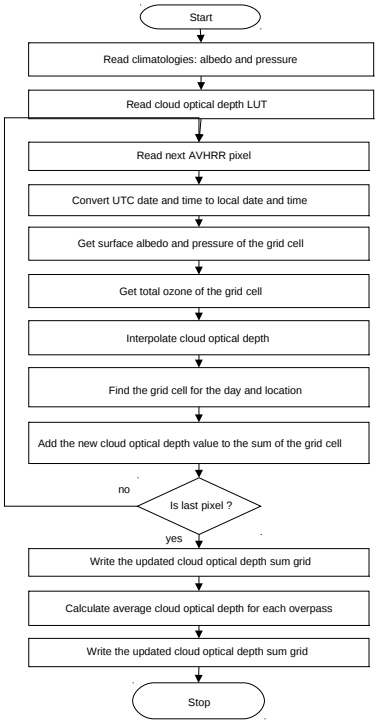

Figure 2.7: Flowchart of the cloud optical depth estimation algorithm. Similarly to the mapping of the ozone data, two files are updated during the process: one containing the sum of cloud optical depths and the number of terms in the sum for each overpass of the grid cells while the other one contains the average cloud optical depth for each overpass of the grid cells.

for this area are determined, and if the difference between the maximum and minimum is larger than a threshold value, the grid cell is flagged as inhomogenous. The threshold value in the current version is 0.1.

2.4.3 Aerosol grid

The aerosol optical depths are obtained from a climatology by S. Kinne [RD21]. This climatology combines various satellite AOD products to a composite that best agrees with AERONET ground-based measurements. The climatology gives the AOD at 550 nm. The water-soluble aerosol model at 0 % humidity (waso00) of the GADS database [RD6] is used to map the AOD to other wavelengths.

2.5 Evaluation of the diurnal integral

The diurnal integral given by eq. 2.3 is evaluated using trapezoidal integration with half an hour time steps from the sunrise to the sunset. The cloud optical depths are first obtained for all AVHRR ground pixels as described in section 2.3. The geolocation and the measurement time of the ground pixel centre are used to collect pixels within a grid cell and belonging to the same AVHRR (onboard Metop or NOAA) overpass. The cloud optical depths of these pixels $\tau_{cld,pxl}$ are averaged to a grid cell average observation $\tau_{cld,obs}(t_{ovp})$ given by

$$\tau_{cld,obs}(t_{ovp}) = \frac{1}{N_{pxl}} \sum_{i_{pxl}=1}^{N_{pxl}} \tau_{cld,pxl}(i_{pxl}) \tag{2.12}$$

where N_{pxl} is the number of pixels and i_{pxl} is the index of the pixel to be averaged. The grid average overpass time t_{ovp} is the average of the measurement times of the individual AVHRR pixels.

The observed cloud optical depths $\tau_{cld,obs}$ are interpolated to the times t_d of the sunlit part of the

diurnal cycle using nearest neighbour interpolation, represented by

$$\tau_{cld}(t_d) = \tau_{cld,obs}(i_{ovp}) \tag{2.13}$$

where i_{ovp} is the index of the overpass closest in time to the diurnal time t_d. This approach avoids the possibly large errors in the cloud observations with large solar zenith angles early in the morning and late in the evening to affect the high dose rate region near noon.

Similarly, the GOME-2 ozone observations are interpolated to the diurnal cycle giving for the grid average ozone vertical column density $N_{v,ozone}(t_d)$

$$N_{v,ozone}(t_d) = N_{v,ozone,obs}(i_{ovp}) \tag{2.14}$$

where $N_{v,ozone,obs}(i_{ovp})$ is the grid cell average ozone column density. With the look-up table given by eq. 3.3, the diurnal integral is evaluated for a given weighting function using the trapezoidal rule as

$$\begin{aligned} H_w &= \int_{t=sunrise}^{sunset} E'_w(t)dt \\ &= 0.5 \sum_{i=0}^{N_d-1} \{LUT_{DSR}(j_w, \theta(t_{d,i}), p, A_s, \tau_{aer}, \tau_{cld}(t_{d,i}), \Omega(N_{v,ozone}(t_{d,i}))) \\ &+ LUT_{DSR}(j_w, \theta(t_{d,i+1}), p, A_s, \tau_{aer}, \tau_{cld}(t_{d,i+1}), \Omega(N_{v,ozone}(t_{d,i+1})))\} (t_{d,i+1} - t_{d,i}) \end{aligned} \tag{2.15}$$

where j_w is the index of the weighting function, N_d is the number of diurnal times, $\theta(t_{d,i})$ is the solar zenith angle at diurnal time $t_{d,i}$ and $\Omega(N_{v,ozone}(t_{d,i}))$ refers to the TOMS V7 ozone and temperature profiles [RD23] interpolated to the given ozone vertical number density and the latitude of the grid cell location. The pressure p, the surface albedo A_s and the aerosol optical depth τ_{aer} are constant during the day. The diurnal times $t_{d,i}$ cover the sunlit part of the day with half an hour intervals from the sunrise to the sunset. The sunrise and sunset are the times when the solar zenith angle is 88 degrees, the largest value in the look-up table.

3 Radiative Transfer Modelling

It is evident from chapter 2 that all the atmospheric physics are in the look-up tables. This chapter describes the look-up tables in more detail.

3.1 Model atmosphere

Figure 3.1 shows the structure of the model atmosphere that is used in all radiative transfer calculations of look-up tables. The first 1 km layer above the surface contains aerosols to capture the effect of scattering and absorbing boundary layer aerosols on the surface UV, while the second 1 km layer contains a cloud to capture the strong effect of cloud scattering to surface UV. Clouds and aerosols are modelled as Mie scatterers. Figure 3.2 shows the cloud and aerosol scattering phase functions as a function of the scattering angle. The aerosol optical depth and surface albedo are taken from climatogies as described in section 2.4.

3.2 Dose rate look-up tables

The hemispherical surface irradiance for unit solar irradiance is calculated by the VLIDORT radiative transfer model [RD8] as a sum of the direct beam contribution and the Gaussian quadrature of the down-

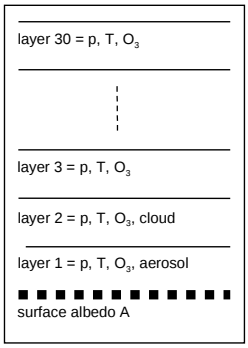

Figure 3.1: The model atmosphere. Above the surface, the first 1 km layer contains aerosol while the second 1 km layer contains cloud. All the 30 layers contain air at pressure p and temperature T, and ozone. The temperature and ozone consentration of each layer are interpolated from the TOMS V7 climatology [RD23].

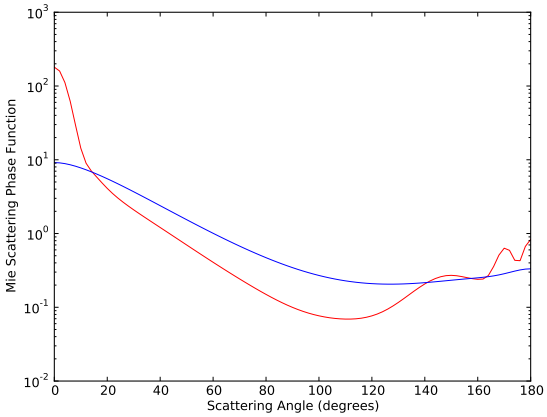

Figure 3.2: The cloud (red) and aerosol (blue) phase functions at 630 nm. The aerosol model is the GADS water-soluble model at 0 % humidity [RD6]. The clouds are modelled as water droplets with a droplet size distribution similar to C1 cloud of Deirmendjian [RD7] with an effective radius of 6 μm. Note the logarithmic scale on the y axis.

welling intensities along the stream directions giving the spectral flux transmittance T_λ

$$T_\lambda = I_{direct} cos\theta + 2\pi \sum_{i=1}^{N} a(i)x(i)I(i) \tag{3.1}$$

where $x(i)$ are the abscissas and $a(i)$ are the weights of the Gauss-Legendre integral and N is the number of streams in the hemisphere. The VLIDORT settings are listed in table 3.3.

The spectral flux transmittance is first (linearly) interpolated to the wavelengths of the extraterrestrial solar spectrum E_0 and then the two are multiplied to give the spectral irradiance on the surface:

$$E_\lambda = E_{0,\lambda} T_\lambda \tag{3.2}$$

After multiplication by each weighting function, the dose rates are calculated from equation 2.2 by trapezoidal integration and stored in the look-up table as

$$LUT_{DSR}(i_w, \theta, p, A_s, \tau_{aer}, \tau_{cld}, \Omega) \tag{3.3}$$

where i_w is the index of the weighting function. The other node points of the look-up table are listed in table 3.1.

3.3 Photolysis frequency look-up tables

Similarly to section 3.2, the spherical irradiance (actinic flux) for unit solar irradiance is calculated by the VLIDORT radiative transfer model [RD8] as a sum of the direct beam contribution and the Gaussian quadrature of the downwelling intensities along the stream directions giving the spherical spectral flux transmittance T_λ^{sphe}

$$T_\lambda^{sphe} = I_{direct} + 2\pi \sum_{up,down} \sum_{i=1}^{N} a(i)I(i) \tag{3.4}$$

where $a(i)$ are the weights of the Gauss-Legendre integral and N is the number of streams in the hemisphere. The VLIDORT settings are listed in table 3.3.

The spherical spectral flux transmittance is first (linearly) interpolated to the wavelengths of the extraterrestrial solar spectrum E_0 and then the two are multiplied to give the spectral irradiance on the surface:

$$E_\lambda = E_{0,\lambda} T_\lambda^{sphe} \tag{3.5}$$

The photolysis frequencies are calculated from equation 2.7 by trapezoidal integration and stored in the look-up table as

$$LUT_{DSR}(i_X, \theta, p, A_s, \tau_{aer}, \tau_{cld}, \Omega) \tag{3.6}$$

where the index of the species i_X is either O^1D or NO_2. The other node points of the look-up table are listed in table 3.1.

3.4 Cloud optical depth look-up table

The upwelling spectral intensity (radiance) I_λ at TOA is calculated with VLIDORT for the node points listed in table 3.2. The VLIDORT settings are listed in table 3.3. The in-band radiance I is then obtained for each AVHRR channel 1 response function R_λ from:

$$I = \int_{\lambda_1}^{\lambda_2} I_\lambda E_{0,\lambda} R_\lambda d\lambda \tag{3.7}$$

The spectral intensity and the channel 1 response functions are linearly interpolated to the wavelengths of the extraterrestrial solar irradiance spectrum before trapezoidal integration of eq. 3.7. The in-band

extraterrestrial solar irradiance is obtained from:

$$E = \int_{\lambda_1}^{\lambda_2} E_{0,\lambda} R_\lambda d\lambda \tag{3.8}$$

and the ratio I/E is stored in the look-up table as:

$$\frac{I}{E}(\tau_{cld}, \phi, \theta, \theta_0, p, \tau_{aer}, A_s, \Omega) \tag{3.9}$$

Table 3.1: Node points of the dose rate and photolysis frequency look-up tables. The TOMS V7 ozone profile climatology [RD23] is used together with the associated temperature profiles.

parameter	symbol	node values
solar zenith angle	θ_0	0, 5, 10, ... 85, 88
pressure	p	0.7, 1.0
surface albedo	A_s	0, 0.1, 0.2, ... 1.0
aerosol optical depth at 500 nm	τ_{aer}	0, 0.1, 0.2, ... 1.0
cloud optical depth at 500 nm	τ_{cld}	0, 0.39, 0.92, 1.7, 2.7, 4.1, 6.1, 8.9, 13, 18, 25, 36, 50, 70, 96, 130, 190, 260, 360, 500
TOMS V7 ozone and temperature profile	Ω	full set

Table 3.2: Node points of the cloud optical depth look-up table. A subset of the TOMS V7 ozone profile climatology [RD23] is used together with the associated temperature profiles. M125, M325 and M575 refer to the middle latitude profiles for total ozone columns of 125, 325 and 575 DU, respectively.

parameter	symbol	node values
wavelength	λ	550, 570, 580, 590, 600, 610, 630, 650, 690, 710, 730, 750
solar zenith angle	θ_0	0, 5, 10, ... 80
satellite zenith angle	θ	0, 5, 10, ... 70
relative azimuth angle	ϕ	0, 20, 40, ... 180
pressure	p	0.7, 1.0
surface albedo	A_s	0, 0.3, 0.6, 1.0
aerosol optical depth at 500 nm	τ_{aer}	0, 0.2, 0.4, 0.6, 0.8, 1.0
cloud optical depth at 500 nm	τ_{cld}	0, 0.5, 1.0, 2.0, 4.0, 8.0, 16.0, 32.0, 64.0, 128.0, 256.0, 500.0
TOMS V7 ozone and temperature profile	Ω	M125, M325, M575

Table 3.3: VLIDORT settings for the surface irradiance and AVHRR channel 1 TOA radiance simulations.

parameter	value for surface irradiance	value for AVHRR ch1 radiance	notes
vlidort option	2	2	option 2 = pseudo spherical calculation for BOA geometry
number of Stokes parameters	1	1	-
number of layers	30	30	-
number of streams	50	20	-
do NT correction	no	yes	NT = Nakajima-Tanaka correction
vlidort accuracy	0.01	0.001	accuracy criterion for Fourier convergence

4 Error sources

The error in the surface UV product depends strongly on the ozone concentration, surface albedo, solar zenith angle, cloud optical depth and the amount UV absorbing aerosols in the atmosphere [RD9]. The errors due to surface albedo, clouds, aerosols and extraterrestial solar irradiance are similar to all products. The integrated UVA and j(NO_2) products are less sensitive to errors in ozone because the strong ozone absorption at wavelengths shorter than 330 nm contribute less to the integral over wavelength. As the product is not given at the overpass time of the satellite, diurnal variation of clouds, aerosols and ozone also contribute to the error budget. The error sources are discussed below in the order of decreasing importance.

4.1 Errors from insufficient cloud data

Large errors in the UV product are encountered if the amount of diurnal cloud data is insufficient. Meerkötter et al. [RD11] have estimated the maximum error in the daily dose as a function of the number of NOAA AVHRR overpasses per day. With only one overpass the error is between 20 and 50 %. A second overpass can reduce the error below 20 % if the two overpasses can appropriately represent the temporal cloud field asymmetry. With three overpasses the error was reduced to ca. 10 %.

4.2 Errors from clouds and surface albedo

The error in the surface UV irradiance is very sensitive to the surface albedo A_s [RD10], especially in the presence of clouds. This effect can be estimated using a simple model of Eck et al. [RD12]:

$$E = \left[\frac{E(A_s = 0)}{1 - A_s S_b}\right]\left[\frac{1 - R_{360}}{1 - A_s}\right] \tag{4.1}$$

where R_{360} is the Lambert equivalent reflectivity at 360 nm obtained by removing the atmospheric scattering component from the measured radiance and S_b is the diffuse reflection of a Rayleigh atmosphere illuminated below by an isotropic source. Taking the derivative with respect to the albedo gives for the relative error in the irradiance [RD10]:

$$\frac{\Delta E}{E} = \left(\frac{S_b}{1 - A_s S_b} + \frac{1}{1 - A_s}\right)\Delta A_s \tag{4.2}$$

Unfortunately, the surface albedo climatology does not contain the error ΔA_s, and therefore, the error has to be estimated. The grid average surface UV albedo is typically order of 5 % for land and 10 % for water. The 0.5x0.5 degree grid cells can contain both water and land. The albedo is then between 0 % and 10 %, i.e. 5 +- 5 % (min/max), indicating that the maximum error for the albedo is 5 %. It is difficult to estimate it for larger albedos and therefore the same number is used. Any BRDF effects are ignored in the current approach. Figure 4.1 (left) shows a plot of the total percent error and the contributing terms for a realistic value of 0.5 for the S_b. At albedo of 0.8, a 5 % error in the albedo translates into a 30 % uncertainty in the surface irradiance. At even larger albedos, the relative error increases rapidly, finally reaching 100 % error per 1 % error in albedo.

Similar errors arise when the cloud correction factor is determined with a radiative transfer model retrieving the optical thickness from the measured radiance. The determination of optical thickness becomes less accurate with increasing surface albedo because the intensity contrast between the surface and the cloud decreases (figure 4.1, right).

4.3 Errors in ozone profile and total column ozone

The surface UV irradiance is sensitive to both the ozone profile and the total column ozone. Because of the Umkehr effect, the dependence is a complex function of the solar zenith angle and the wavelength.

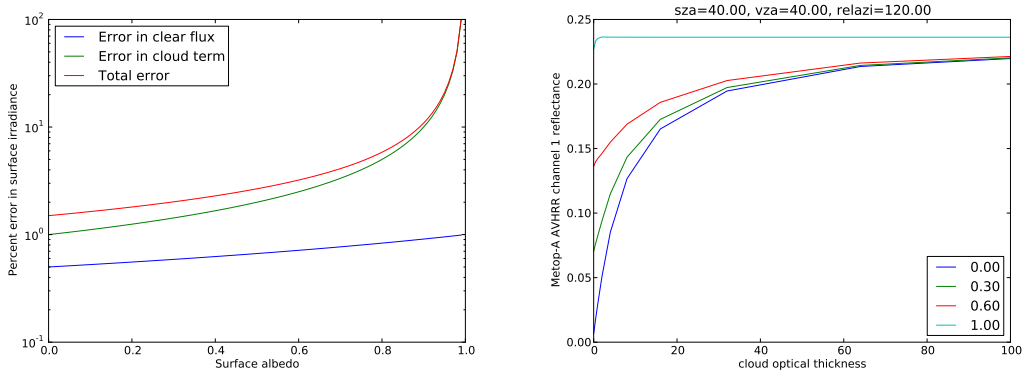

Figure 4.1: Left: percent error in surface UV irradiance for unit error in surface albedo. The increase of the total error (red) with surface albedo is dominated by the error in the cloud term (green) while the clear flux term increases only slightly. Right: typical dependence of the AVHRR channel 1 reflectance on cloud optical thickness for different surface albedos.

Krotkov et al. [RD9] have studied these effects in detail. The results indicate that a 10 DU error in the total column ozone translates into 2-6 % error at 310 nm, 10-16 % at 300 nm and 20-30 % at 295 nm. In addition, the total column ozone varies during a day affecting the determination of the daily dose. A reasonable estimate for the maximum error due to total column ozone is 15 % (5 % std).

The sensitivity to the ozone profile is weak for small solar zenith angles, but at angles larger than 70 degrees the sensitivity becomes more significant. Based on the results of Krotkov et al. [RD9], the maximum error in the irradiance can be estimated as 3 % for solar zenith angles smaller than 70 degrees and 15 % for larger angles.

4.4 Errors from UV-absorbing aerosols

The sources of UV absorbing aerosols are urban pollution, biomass burning and desert dust. The error can range from a few percent overestimations to 50 % or more depending on the amount of UV absorbing aerosols at the given location [RD9]. According to Herman et al. [RD13], the maximum UV-absorbing aerosol content occurs during June and July when aerosols with an optical depth of at least 0.1 cover about 10 % of the Earth's surface. In these regions, such as the Saharan Desert, a bias of 10 % or more is translated into the UV product if the aerosols are ignored.

4.5 Error in the extraterrestrial solar irradiance

The current processor uses solar irradiance spectrum measured by the SUSIM instrument on the ATLAS-3 mission in April 1994. A conservative estimate for the error in the absolute solar irradiance is 3 % [RD9]. The variation of solar irradiance with the Sun-Earth distance d is taken into account by:

$$E = \frac{E_0(d = 1AU)}{d^2} \tag{4.3}$$

4.6 Total error budget

Table 4.1 summarizes the contributions from the different error sources. This table only includes the error sources that are related to the retrieval of the surface UV product from the satellite measurements. When comparing the product with ground-based measurements additional errors arise from the differences between the two types of measurement. The satellite instrument integrates over a large area, and therefore averages out all cloud and albedo effects, whereas the ground instrument reacts to the passing of every single cloud and is sensitive to the local environment (snow, aerosols etc.). The accuracy requirements (RMS difference between the product and ground-based measurement) for the product are [AD1]:

threshold 50 %, target 20 % and optimal 10 %. From the total error budget of table 4.1 we can see that the optimal value of 10 % requires very accurate data on aerosols, cloud optical depth and albedo. The target value of 20 % is possible if the aerosols are well known. Finally, the threshold of 50 % should be achieved even with climatological aerosol and surface albedo data for regions where the surface albedo is below 0.8.

Table 4.1: Total error budget.

Error Source	Max error (taken as 3 sigma) (%)	Standard deviation (%)
Number of overpasses in cloud retrieval	10 - 50	3 - 17
Albedo and clouds (5 % error in albedo)		
albedo < 0.8	30	< 10
albedo > 0.8	30 - 500	10 - 200
Total column ozone	15	< 5
Ozone profile		
solar zenith angle < 70	3	< 1
solar zenith angle > 70	< 15	< 5
Aerosols	100	< 30
Extraterrestial solar irradiance	9	< 3

A Weighting functions

The CIE erythemal weighting function is

$$W(\lambda) = \begin{cases} 1.0 & \text{when } 250 \leq \lambda \leq 298 \text{ nm} \\ 10^{0.094(298-\lambda)} & \text{when } 298 < \lambda \leq 328 \text{ nm} \\ 10^{0.015(139-\lambda)} & \text{when } 328 < \lambda \leq 400 \text{ nm} \end{cases} \quad \text{(A.1)}$$

The DNA damage weighting function is

$$W(\lambda) = \frac{e^{13.82(\frac{1.0}{D}-1.0)}}{0.0326} \text{ with } D = 1.0 + e^{\frac{\lambda-310}{9}} \quad \text{(A.2)}$$

where normalization to 1.0 at 300 nm is used (normalization to 265 nm is divided by 0.0326). The generalized plant response weighting function is

$$W(\lambda) = \frac{2.618}{0.2176}\left[1.0 - \left(\frac{\lambda}{313.3}\right)^2\right] e^{-\frac{\lambda-300}{31.08}} \quad \text{(A.3)}$$

where normalization to 1.0 at 300 nm is used (normalization to 280 nm is divided by 0.2176).

Table A.1: Action spectrum for the conversion of 7-dehydrocholesterol to previtamin D_3 in human skin, normalized to 1 at 298 nm. Note that the data at wavelengths longer than 315 nm are the result of a mathematical extrapolation and are not based on experimental data. From ref. [RD5].

Wavelength [nm]	Relative response [unitless]	Wavelength [nm]	Relative response [unitless]
252	0.036	292	0.928
253	0.039	293	0.952
254	0.043	294	0.976
255	0.047	295	0.983
256	0.051	296	0.990
257	0.056	297	0.996
258	0.061	298	1.000
259	0.066	299	0.977
260	0.075	300	0.951
261	0.084	301	0.917
262	0.093	302	0.878
263	0.102	303	0.771
264	0.112	304	0.701
265	0.122	305	0.634
266	0.133	306	0.566
267	0.146	307	0.488
268	0.160	308	0.395
269	0.177	309	0.306
270	0.195	310	0.220
271	0.216	311	0.156
272	0.238	312	0.119
273	0.263	313	0.083
274	0.289	314	0.049
275	0.317	315	0.034
276	0.346	316	0.020
277	0.376	317	1.41E-02
278	0.408	318	9.76E-03
279	0.440	319	6.52E-03
280	0.474	320	4.36E-03
281	0.543	321	2.92E-03
282	0.583	322	1.95E-03
283	0.617	323	1.31E-03
284	0.652	324	8.73E-04
285	0.689	325	5.84E-04
286	0.725	326	3.90E-04
287	0.763	327	2.61E-04
288	0.805	328	1.75E-04
289	0.842	329	1.17E-04
290	0.878	330	7.80E-05
291	0.903		